Georgia Journal of Science

Volume 78 *No. 2 Scholarly Contributions from the Membership and Others* Article 14

2020

Characteristics of Alfvén waves with nonzero k⊥ values

Dereth Drake
Valdosta State University, djdrake@valdosta.edu

Joshua D. Rhudy
Valdosta State University, rdrhudy@valdosta.edu

Brian Shanken
Valdosta State University, bcshanken@valdosta.edu

CHARACTERISTICS OF ALFVÉN WAVES WITH NONZERO $K_\perp$ VALUES

Dereth J. Drake
Joshua D. Rhudy
Brian C. Shanken
Department of Physics, Astronomy, Geosciences and Engineering Technology
Valdosta State University
Valdosta, Georgia, United States of America
djdrake@valdosta.edu

ABSTRACT

Turbulent interactions between Alfvén waves are a common occurrence in astrophysical plasma environments. Many experiments have been conducted to understand these interactions. In this paper, we describe an experiment for the collision of two counterpropagating Alfvén waves. The magnetic and electric field data from the collision is used to determine the energy density and the energy flux density (or Poynting vector) for the waves. Additionally, we discuss some interesting results from a measurement of the Alfvén speed when at least one of the Alfvén waves in the experiment has multiple, nonzero $\mathbf{k}_\perp$ values.

Keywords: Alfvén speed, Alfvén wave, energy density, turbulence, energy flux density, Poynting vector, Elsässer probe, Large Plasma Device

1. INTRODUCTION

In most introductory physics and astronomy courses, students are introduced to the electromagnetic spectrum, sometimes referred to as Maxwell's rainbow. The spectrum goes from very short wavelength, high frequency waves, such as gamma rays and x-rays, to long wavelength, low frequency waves, such as radio or microwaves. Electromagnetic waves are transverse, propagating waves that carry energy through space without requiring a medium to travel through. However, as the waves travel through interstellar space, they encounter different astrophysical environments, most of which are in a plasma state (Yiğit 2017).

A plasma is a gas that has been ionized such that there are many ions and free electrons in a specific area of space such that the system is electrically neutral (see Chen 1984). The length of that area the plasma covers must be much greater than the Debye length, or the distance around a charged particle where the particle no longer can influence another charged particle nearby. Additionally, unlike a gas, plasmas exhibit collective behavior where a small change in one area of the system can cause a rippling effect throughout the entire plasma system. When an electromagnetic wave enters a plasma region, the electrons and ions within the plasma can be affected by the presence of the wave. This interaction can produce subsequent waves known as magnetohydrodynamic (MHD) waves. The type of MHD wave produced depends on if the wave is longitudinal or transverse and if the wave is traveling parallel or perpendicular to the background magnetic field of the plasma.

When an MHD wave is produced that is both longitudinal and is traveling parallel to the background magnetic field, this wave is referred to as an Alfvén wave. First predicted by Hannes Alfvén in 1942 (Alfvén 1942), Alfvén waves typically have very long wavelengths, on the order of hundreds of kilometers, and very low frequencies. These waves have been observed in the Earth's ionosphere (Papadopoulos et al. 1982; Louarn et al. 1994), the solar corona (Tomcyk et al. 2007), the solar wind (Unti and Neugebauer 1968), and the interplanetary medium (Belcher and Davis 1971; Velli et al. 1989). In addition, these waves have also been observed in many terrestrial plasma devices, such as tokamaks (Appert et al. 1982; Fuchs et al 1995; Huasen and Zhihong 2013) and helical plasma chambers (Kolesnichenko et al 2004; Toi et al 2011; Ogawa et al 2012).

As with any other type of wave, Alfvén waves can interact with each other through collision to produce additional effects in the plasma environment. Many theories and experiments have been developed to study the interactions between Alfvén waves in these various environments (Carter et al. 2006; Howes et al. 2012; Drake et al. 2013). The turbulent interaction of counterpropagating Alfvén waves has been shown to explain electron acceleration leading to the auroras in the northern hemisphere of Earth (Birn et al. 2012; Schroeder et al. 2017), typically referred to as the aurora borealis. Additionally, counterpropagating Alfvén waves have been proposed to explain the coronal heating problem for the sun (van der Holst et al. 2014). This problem comes from the fact that the corona is significantly warmer than the chromosphere, 500,000 K and 8,000 K, respectively. The change in temperature happens in such a short distance (~100 km) that typical heating mechanisms that are taught in thermodynamics courses cannot explain the process. However, the presence of interacting Alfvén waves has been shown to explain this extreme change in temperature.

Although there has been a lot of research conducted on Alfvén waves, there is still much that has yet to be understood about this type of MHD wave. One particular piece of information that seems to be absent from the literature is the measurement of the Poynting vector and energy density during the collision between two Alfvén waves. In this paper we measure these values by through an experiment in which two counterpropagating Alfvén waves are launched along a magnetically confined plasma column, where one of the waves have a nonzero wavenumber ($\mathbf{k}$). In Section 2 we present the theory for calculating the energy density and energy flux density as well as the Alfvén speed with a wave has a nonzero $\mathbf{k}_\perp$ value. Section 3 describes the experiment conducted and a little-known tool (the Elsässer probe) that can be used to simultaneously measure the magnetic and electric fields for propagating Alfvén waves. Experimental data is used to determine the speed of the Alfvén waves using two different methods and comparison of the results is given in Section 4.2. Finally, in Section 4.3, we discuss the results of the calculation of the energy density and Poynting vector at the interaction of two waves and what that data indicates about both parameters in turbulent interactions.

2. THEORY

For most electromagnetic waves, the electric field and magnetic field are related by $\mathbf{E}/\mathbf{B} = c$, where c is the speed of light. This equation works well for any electromagnetic wave traveling through a vacuum. But inside of a plasma, c is replaced by the group velocities (V_g) in order to account for the plasma effects, where the group velocity is defined as the speed of the overall wave packet instead of the individual oscillations within each packet. Alfvén waves are characterized by having a group velocity ($V_g = V_A$) which

can be determine by $V_A = \mathbf{B}_0/\sqrt{\mu_0\rho_0}$ (Allen et al. 1959). Here $\mathbf{B}_0$ is the background magnetic field in the plasma, μ_0 is the permeability of free space, and ρ_0 is the plasma mass density. All quantities in this paper are measured in Gaussian cgs units, unless otherwise stated, as per the NRL plasma formulary (NRL 2019).

Another property of any wave is the wavenumber. The wavenumber is defined as the total number of wavelengths per unit distance, or $k = 2\pi/\lambda$. In a plasma environment, the wavenumber will split into two components, one parallel to the wave's direction of motion ($\mathbf{k}_{||}$) and one perpendicular ($\mathbf{k}_\perp$) to the motion. One of the problems with the equation for the group velocity of an Alfvén wave (V_A) is that it only works well when the perpendicular wave number, $\mathbf{k}_\perp$, is very close to zero (Gekelman et al. 1997). So, at larger values of the $\mathbf{k}_\perp$, a correction factor (C_{cf}) must be included in the calculation.

To determine the correction factor, the equations for magnetohydrodynamics can be used since they allow for the study of the evolution of an MHD wave in a plasma environment. If the wave speed is substituted with the Alfvén speed, then the MHD equations simplify down to a symmetric set of equations for the motion of a wave traveling up (z^-) the magnetic field or down the magnetic field (z^+; Elsässer 1950),

$$\frac{\partial z^\pm}{\partial t} \mp V_A \cdot \nabla z^\pm + z^\mp \cdot \nabla z^\pm = \frac{\nabla p}{\rho_0}. \tag{1}$$

Here p is the thermal pressure, $\boldsymbol{z}^\pm = \mathbf{v} \pm \delta\mathbf{B}/\sqrt{\mu_0\rho_0}$, $\mathbf{v}$ is the wave speed, and $\delta\mathbf{B}$ is the fluctuating part of the magnetic field (here after referred to as the magnitude of the magnetic field). Substituting in the fluid velocity for a plasma, $\mathbf{v} = C_{cf}\,\mathbf{E}\times\mathbf{B}_0/\mathbf{B}_0^2$, for the wave speed, we can see that

$$z^\pm = C_{cf}\frac{\mathbf{E}\times\mathbf{B}_0}{\mathbf{B}_0^2} \pm \frac{\delta\mathbf{B}}{\sqrt{\mu_0\rho_0}}. \tag{2}$$

Normalizing with respect to $V_A\boldsymbol{B}_0$, we can obtain a relationship for the Alfvén speed to the same correction factor,

$$V_A = C_{cf}\frac{E}{\delta B}. \tag{3}$$

Then by specifying, without loss of generality, that the linear wave vector for an Alfvén wave is $\mathbf{k}_\perp = k_x\hat{x} + k_z\hat{z}$ and that the background magnetic field is given by $\mathbf{B}_0 = B_0\hat{z}$, we can obtain the correction factor for a wave traveling along the z-axis of a plasma column, as discussed in Gekelman et al. (1997),

$$\frac{1}{C_{cf}} = \pm\sqrt{\left(1 + {k_x}^2{\delta_e}^2\right)\left(1 - \omega^2/{\Omega_i}^2\right)}. \tag{4}$$

Here ω is the plasma frequency determined from

$$\omega = 5.64 \times 10^4\sqrt{n_e}, \tag{5}$$

δ_e is the electron skin depth given, or the depth to which an external electromagnetic wave can penetrate the plasma, by

$$\delta_e = 5.31 \times 10^5 / \sqrt{n_e}, \tag{6}$$

and Ω_i is the ion cyclotron frequency, as determined from

$$\Omega_i = Ze|B_0|/m_i. \tag{7}$$

Here Z is the ion charge state, e is the charge of the electron, and m_i is the mass of the ion species.

As with other electromagnetic and MHD waves, the Alfvén wave stores energy (U) in its electric and magnetic field components. In free space, where $V_g = c$, the energy is carried half by the electric field and half by the magnetic field. However, in a plasma environment this is not always the case. Since the stored energy will be spread over the entire wave, the energy density (u) is more useful to look at then the stored energy (U). The energy density, or the energy per unit volume (V), is given by

$$u = \frac{U}{V} = \frac{1}{2}\left(\varepsilon_0 \mathbf{E}^2 + \frac{\mathbf{B}^2}{\mu_0}\right), \tag{8}$$

where **E** is the electric field component of the wave, ε_0 is the permittivity of free space, and **B** is the magnetic field component of the wave. This value will allow us to see how much energy is actually being transported by the wave.

Another useful parameter when looking at energy is the Poynting vector (**S**), also referred to as the energy flux density. Since power is the rate of change of the energy in the system per unit time, **S** can be used to determine how the energy within an electromagnetic wave is being transported. In other words, the Poynting vector is the power transported by the wave through an area of space. If **S** is large, then the power is able to be transported easily over large distances without loss of energy into the surrounding environment. If **S** is small, then the power carried by the wave will be lost to the plasma environment. The Poynting vector is determined by (Volwerk et al. 1996)

$$\mathbf{S} = \frac{1}{\mu_0}(\mathbf{E} \times \mathbf{B}). \tag{9}$$

3. EXPERIMENTAL APPROACH

The experiment was conducted in the Large Plasma Device (LaPD) at UCLA, a picture of the device can be seen in Figure 1. The LaPD is a 20 m long evacuated, cylindrical chamber surrounded by solenoids (purple and yellow in the picture) that are capable of producing magnetic fields up to 2500 G (Gekelman et al. 1991; Leneman et al. 2006). A barium-oxide coated cathode is located at one end of the chamber and, in conjunction with an anode mesh, is able to produce a magnetically confined plasma of about 16.5 m in length with diameters of 40 to 70 cm. Because the shot-to-shot variation in the plasma is extremely low, data can be taken by averaging over 10 shots to produce a high signal-to-noise ratio (Drake et al. 2013).

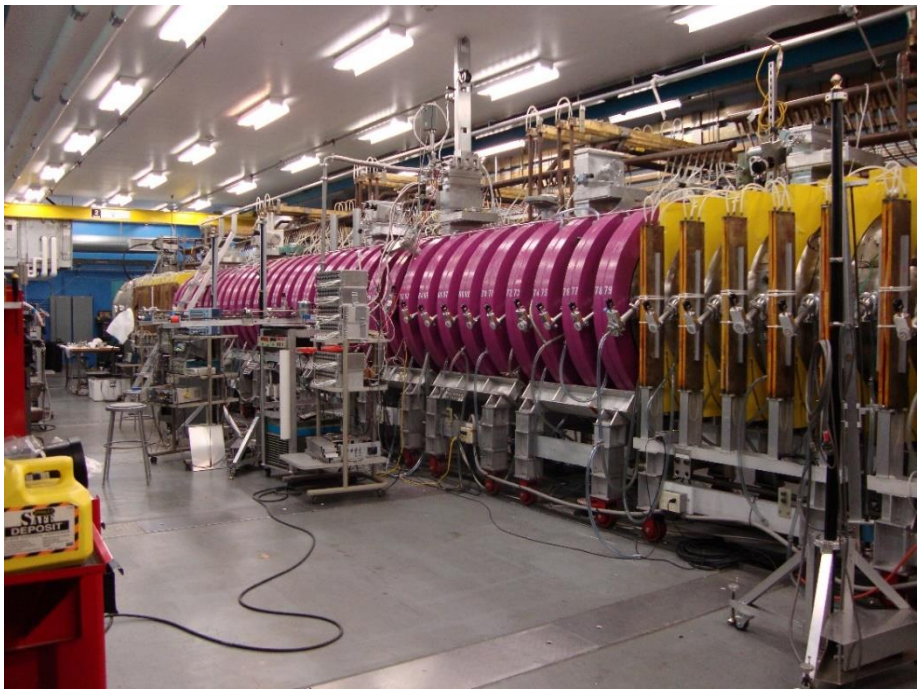

Figure 1. A picture of the Large Plasma Device at UCLA taken by the authors.

The experiment was conducted in a 50% mixture of helium and hydrogen. The background magnetic field was set to B_o = 1800 G. We used a Langmuir probe (Chen 1965) to measure the electron temperature and plasma density. The Langmuir probe consists of one wire electrode, which has been biased with a voltage that can be swept upward and the current produced on the probe is then measured. Using a plot of current versus voltage and equation (2) from Chen (1965), we can determine the different plasma parameters. For the experiment presented here, we measured the electron temperature to be T_e = 7.0 eV and a plasma density of $n_e = 1.25 \times 10^{12}$ cm^{-3}.

Two Alfvén wave antennas were inserted into the plasma perpendicular to the plasma column separated by a distance of 15 m (Figure 2). The first antenna is known as the Iowa arbitrary spatial waveform (ASW) antenna and it consists of 48 copper meshes spaced over an area of 30.5 cm × 30.5 cm (Kletzing et al. 2010). Each grid element is driven separately and can be adjusted to a maximum or minimum multiplicative value of 1 or -1. The result is a small amplitude Alfvén wave that varies in the x-direction with little variation in the y-direction. This means that the value of the perpendicular wave number will be greater in the x-direction then in the y-direction. The ASW antenna is capable of being tuned to a specific k_x value allowing for selection of nonzero k_x values for the Alfvén wave. For this experiment we tuned the antenna to produce a k_x = 0.6 cm^{-1} wave.

The second antenna is the UCLA loop antenna (Auerbach et al. 2011). This antenna has two overlapping rectangular loops that are 21.5 cm × 29.5 cm. The loops are positioned such that they make an X shape on the end, as indicated in the diagram. By ensuring that the loops are perpendicular to each other and varying the phase of each loop's signal, a large amplitude Alfvén wave that varies in the y-direction is produced. Since the antenna has little deviation in the x-direction, k_y = 0.1 cm^{-1} and $k_x \sim 0$.

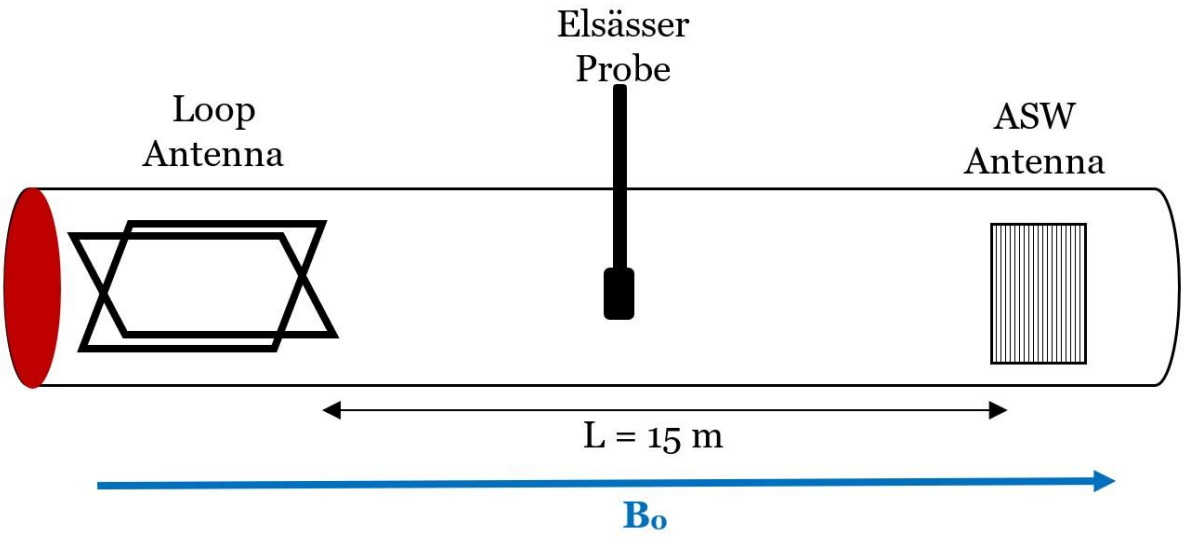

Figure 2. Schematic for the Alfvén wave collision experiment.

An Elsässer probe (Drake et al. 2011) was used to make simultaneous measurements of both the electric and magnetic components of the Alfvén waves. To measure the magnetic field component, a thin coil of wire is wrapped tightly around a ceramic stock and placed at the end of a larger ceramic tube, as shown in Figure 3. The red and green loops on the end indicate the location of the B-dot probes for the B_x and B_y components of a traveling Alfvén wave. When a time varying magnetic field passes through the coil, a current is produced in the wire. Measuring the induced current (i) and using Faraday's law, see equation (10), the magnitude of the magnetic field can be determined (Mirnov 1964).

$$iR = \varepsilon = -\frac{d\varphi}{dt} \tag{10}$$

Here ε is the induced potential in the probe, R is the internal resistance of the probe, and $\varphi = \int B \cdot dA$. The coil is often referred to as a B-dot probe since it measures the time varying magnetic field and not the magnetic field directly.

Figure 3. A three-dimensional CAD model of the Elsässer probe. The red and green loops on the end indicate the location of the B-dot probes for the B_x and B_y components of a traveling Alfvén wave. Gray wires show the relative position of the electric field probes. The total length is approximately 2 cm.

For the electric field, two sets of dipole antennas are placed along the larger ceramic stalk allowing for simultaneous measurements of E_x and E_y by applying $E_r = \Delta V/\Delta r$, where ΔV is the measured potential difference and Δr is the distance between the dipoles loops in either the x or y direction. The gray wires shown in Figure 3 give the relative

position of the electric field probes. The total length from tip of the first B-dot coil to end of the second electric field probe is approximately 2 cm. The probe was calibrated previously in the paper by Drake et al. (2011).

4. DATA ANALYSIS AND DISCUSSION

Using the Elsässer probe, we measured several characteristic quantities of the Alfvén waves produced by both the ASW and loop antennas. The four quantities presented in this paper are the oscillating magnetic field components, speed of the wave, energy density, and Poynting flux.

4.1 Measurements of Magnetic Fields

We first measured the magnetic field of the wave by using the B-dot probe. The magnetic field in the y-direction (B_y) of the propagating wave for the ASW antenna is shown in Figure 4(a) and 4(b). Figure 4(a) gives a two-dimensional plot of the magnetic field at a time of t = 10.242 ms, where the wave's direction of propagation is in and out of the page. The figure shows that the magnetic field (measured in milligauss) varies very little in the spatial y-direction but the amplitude alternates almost uniformly in the x-direction. In Figure 4(b), we see the magnetic field as it propagates through time at the spatial coordinate of y = 0 cm. As with Figure 4(a), this one shows an almost uniform oscillation in the amplitude of the magnetic field of the propagating Alfvén wave from -25 mG to +25 mG.

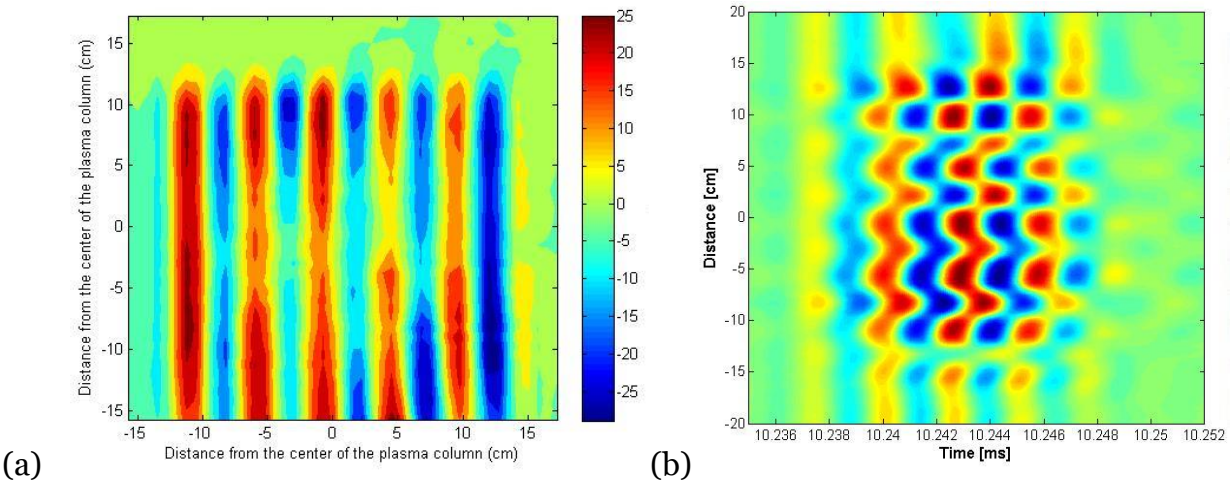

Figure 4. (a) The two-dimensional spatial plot of measured magnetic field B_y (in milligauss) at time t = 10.242 ms and (b) a plot of the B_y as a function of distance and time at the location of y = 0 cm.

The magnetic field for the loop antenna is shown in Figure 5 (measured in Gauss). As can be seen from the figures, the loop antenna varies from -2.5 G to 5.25 G in the x-direction. The figure shows that the magnetic field varies very little in the spatial x-direction, from -2.5 G to 1.5 G, but alternates almost uniformly in the y-direction. Both the B_x component of the ASW antenna and the B_y component of the UCLA antenna are

negligible in comparison to the other component. As such, the k_y and the k_x components for the ASW antenna and UCLA antenna, respectively, are also negligible.

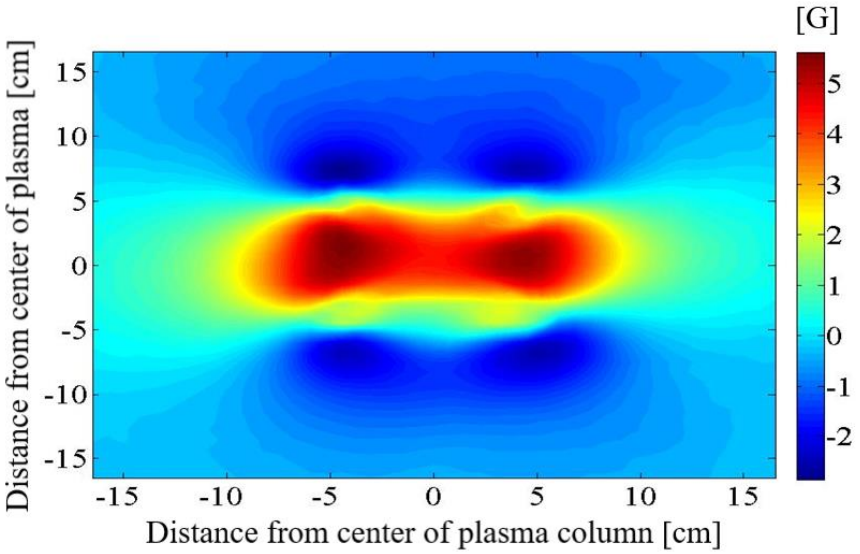

Figure 5. The figure shows the B_x component of the Alfvén wave created by the loop antenna.

4.2 Calculation of Alfvén Speed

One of the benefits of using the ASW antenna is that you can tune the antenna to a particular k_x value. The antenna was tuned to produce a k_x = 0.6 cm^{-1} wave. After taking measurements of both the electric and magnetic fields, a spatial Fourier transform was applied to the data to determine the $\mathbf{k}_\perp$ value (Drake et al. 2013). We found that there were two distinct k_x values for our wave, k_x = 0.2 cm^{-1} and k_x= 0.6 cm^{-1}. Separating the two waves in k-space, an inverse Fourier transform was performed on the data to determine the waves magnetic field for each of the k-values. As shown in Figure 6, the wave's energy was split with 90% at 0.2 cm^{-1} and 10% at 0.6 cm^{-1}. This is a common problem for antennas that work with higher k_x values since most of the energy will be transferred into any lower k_x values produced by the antenna. Note that the times are different in the data because the results were measured in two consecutive data runs.

Using $V_A = \mathbf{B}_0/\sqrt{\mu_0\rho_0}$, the theoretical value for the Alfvén speed was determined to be 2.26 × 10^{10} cm/s. From equations (3) and (4), we found that for the k_x = 0.2 cm^{-1} wave the experimental speed was 1.83 ± 0.3 × 10^{10} cm/s and for the k_x = 0.6 cm^{-1} wave the experimental speed was 2.09 ± 0.4 × 10^{10} cm/s. This is an error of 19% and 7.5%, respectively. Other experiments have been conducted with single nonzero k_x values and the results have indicated very good agreement (<5%) between the theoretical value and the value obtained from the correction factors (Drake et al. 2011). However, it is clear from this experiment that when the wave splits into multiple nonzero $\mathbf{k}_\perp$ values, the method produces a difference between the two results with only the higher $\mathbf{k}_\perp$ value producing a close result with the theoretical value. To first order (one significant figure), we can see that the numbers are very close for both $\mathbf{k}_\perp$ values. However, this loss of precision is not acceptable for most complex models for Alfvén waves and thus the accuracy and precision of the results need to be much greater. This result represents the first measurement of the Alfvén speed, or group velocity, for a wave containing multiple non-zero $\mathbf{k}_\perp$ values.

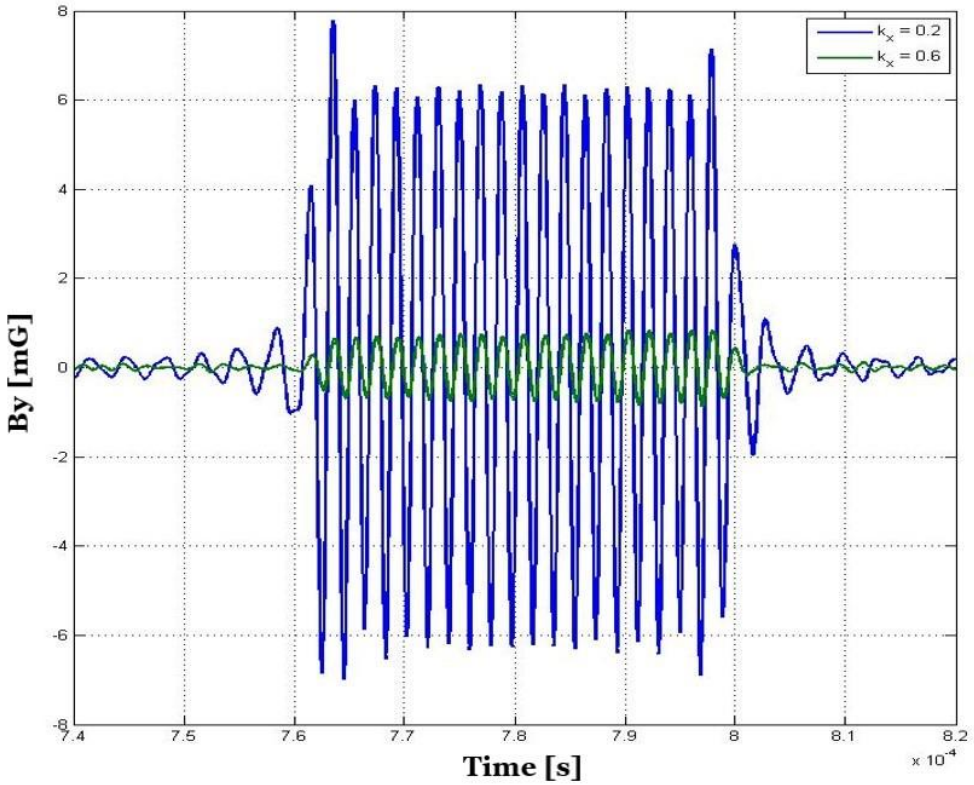

Figure 6. The measured magnetic field of the two known k_x values in this experiment. The wave's energy is split between the two values with 90% at 0.2 cm^{-1} and 10% at 0.6 cm^{-1}.

4.3 Measurements of Energy Density and Poynting Vector

Using the measured electric and magnetic field components, the energy density was calculated from equation (8). Figure 7 shows the energy density from three different data runs. The red graph is the energy density when only the loop antenna was present. In black, we show the energy density when only the ASW antenna is present. In both cases we can see that the energy density of the wave oscillates periodically with the ASW signal significantly smaller, $u = 0.2 \pm 0.04$ J/m^3, than that of the loop antenna with an energy density maximum of $u = 1.4 \pm 0.2$ J/m^3. As can be seen most clearly from the ASW antenna graph, both waves carry energy through the plasma region since the increase is only present at the same time the wave is present.

The blue graph shows when both antennas are on at the same time, i.e. simultaneously launching Alfvén waves. Here we observe a strong increase in the energy density when the two waves interact with an almost doubling in the magnitude of the energy density. Using the Elsässer probe, we also mapped a two-dimensional plot of the energy density over the entire region where the two antennas are in the plasma, Figure 8. In this figure we observe that the energy density has peaks at four distinct points in the plasma column. These four points correspond exactly to the location of the four corners of the loop antenna. This indicates that the two antennas produce some type of resonance effect causing a substantial increase in the energy density. Thus, the turbulent interaction due to the interaction of the two waves has no observable effect on the energy density of either wave.

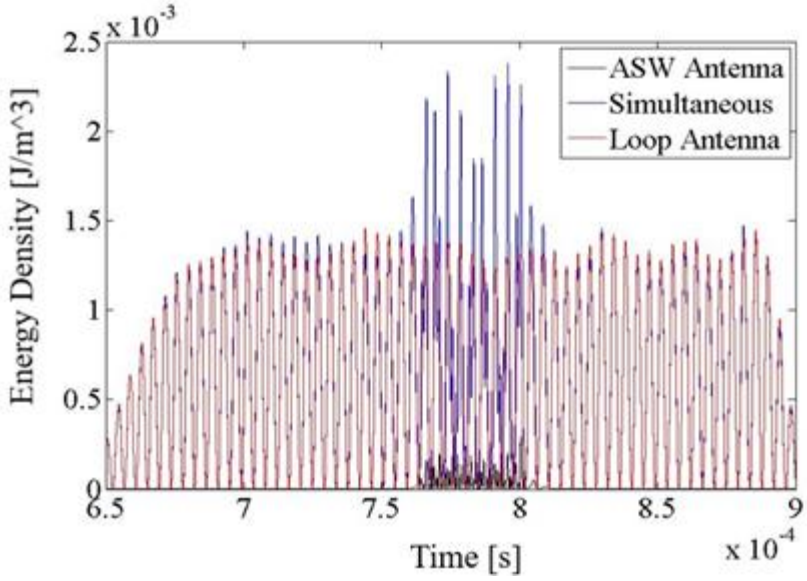

Figure 7. Overlapping plot of the energy densities from three data runs: ASW only (black), the loop antenna only (red), and both on simultaneously (blue). The spike in the middle of the figure (blue) shows an increase in energy density when both waves are propagating in the plasma.

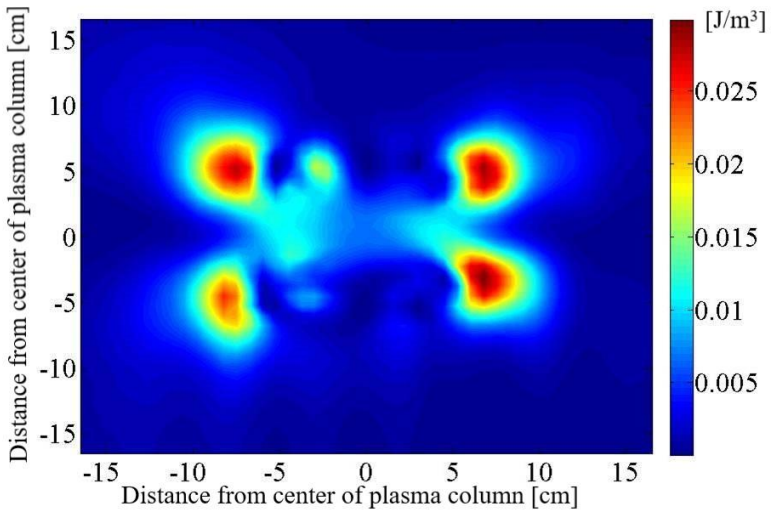

Figure 8. A contour plot of a 30 cm × 30 cm area in the discharge when both antennas are launching Alfvén waves simultaneously. The location x = 0 cm, y = 0 cm is in the middle of the plasma chamber.

The Poynting vector was determined by applying equation (9) to the same data as the energy density. Looking at the same location in the plasma as in Figure 7, we see in Figure 9 that the ASW antenna produces a much larger Poynting vector than the loop antenna. This means that although the ASW antenna generates a much smaller wave, because it is so compact, it is much better at transporting the energy through the plasma column than the loop antenna. This indicates that the energy from this Alfvén wave produced by the ASW antenna can be transported further even at relatively lower intensity without significant losses.

We also observe in the figure that, unlike the case of the energy density, there is no overall increase in the Poynting vector data when the two interact. These observations indicate that the Poynting vector is not modified by the turbulent interaction of counter propagating Alfvén waves, just as in the case of the energy density In addition, using basic physics, and without loss of generality, we can state that the Poynting flux of the daughter wave is a linear combination of that produced by the interaction of the two antennas

Alfvén waves. This result represents the first time this measurement and calculation has been conducted for two counterpropagating Alfvén waves.

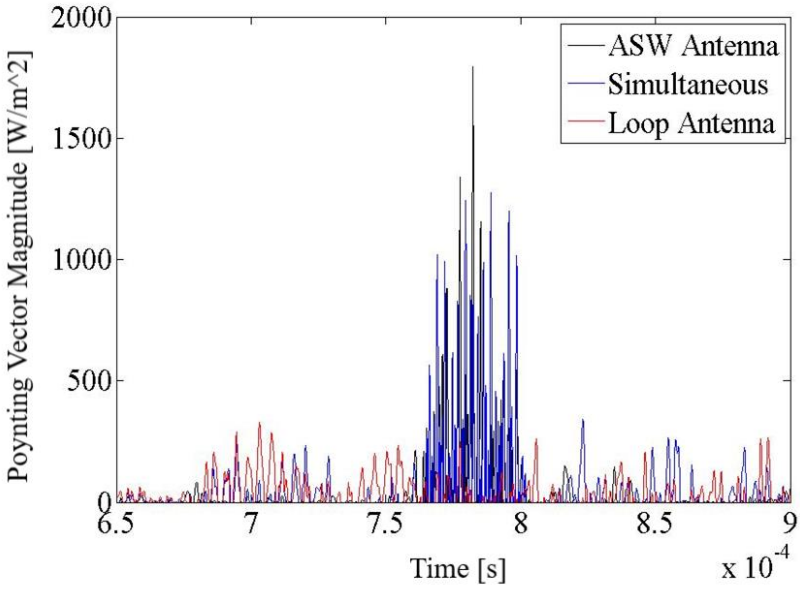

Figure 9. Overlapping plots of the Poynting vector from three data runs described in Figure 7.

5. CONCLUDING REMARKS

Although the main focus of this experiment was not on the Alfvén speed, we found some interesting results for our experiment. The speed is often approximated from $V_A = \mathbf{B}_0/\sqrt{\mu_0\rho_0}$. This equation works very well for environments were the perpendicular wave number is very close to zero. At larger values of $\mathbf{k}_\perp$, a correction factor can be employed to determine the Alfvén speed. However, if the wave splits into multiple nonzero $\mathbf{k}_\perp$ values, as in our experiment, then the current theory and subsequent equations, equations (3) and (4), can only give a first order approximation of the Alfvén speed. As such, a more detailed theory needs to be determined for Alfvén waves with multiple nonzero $\mathbf{k}_\perp$ values. The results presented in this paper are the first measurement of the Alfvén speed, or group velocity, for a wave containing multiple nonzero $\mathbf{k}_\perp$ values.

The energy density and Poynting vector were both determined in this experiment based on the measured magnetic and electric field components from an Elsässer probe. When the energy density was measured for the two-wave interaction, an increase in density was observed only when the two antennas launched waves simultaneously. In Figure 8, we showed a 2-D spatial plot of the energy density for the experiment. This plot indicated that the increase in energy density is more likely to do with a resonant interaction between the antennas instead of an interaction between the two waves themselves. For the energy flux density, we saw that there was little change in the magnitude of the Poynting vector during the turbulent interaction. We also observed that the ASW antenna produced a much more compact and higher intensity Poynting vector over the UCLA loop antenna. This indicates that the ASW antenna is able to transport its energy without much loss of power over the length of the plasma chamber. On the other hand, the loop antenna, which has a much higher magnetic field, loses much of its power as it travels along the plasma column. Thus, we can conclude that during the interaction

of two Alfvén waves, under the conditions identified in this paper, one wave has little to no impact on the energy density or energy flux density (Poynting vector) of the other wave.

REFERENCES

Alfvén, H. 1942. Existence of electromagnetic-hydrodynamic waves. Nature (London), 150, 405–406, doi:10.1038/150405d0.

Allen, T.K., W.R. Baker, R.V. Pyle, and J.M. Wilcox. 1959. Experimental generation of plasma Alfvén waves. Phys. Rev. Lett., 2, 383–384.

Appert, K., R. Gruber, F. Troyuon, and J. Vacalvik. 1982. Excitation of global eigenmodes of the Alfvén wave in tokamaks. Plasma Phys., 29, 1147–1160.

Auerbach, D.W., T.A. Carter, S. Vincena, and P. Popovich. 2011. Control of gradient-driven instabilities using shear Alfvén beat waves. Phys. Plasmas, 18, 055708, doi:10.1063/1.3574506.

Belcher, J.W. and L. Davis. 1971. Large-amplitude Alfvén waves in the interplanetary medium. J. Geophys. Res., 76, 3534–3563.

Birn, J., A.V. Artemyev, D.N. Baker, M. Echim, M. Hoshino, and L.M. Zelenyi. 2012. Particle acceleration in the magnetotail and aurora. Space Sci. Rev., 173, 49–102.

Carter, T.A., B. Brugman, P. Pribyl, and W. Lybarger. 2006. Laboratory observation of a nonlinear interaction between shear Alfvén waves. Phys. Rev. Lett., 96 155001(4).

Chen, F.F. 1965. *Electric Probes in Plasma Diagnostic Techniques*. Eds. R.H. Huddlestone and S.L. Leonard, Academic Press, pg 113–200.

Chen, F.F. 1984. *Introduction to Plasma Physics and Controlled Fusion*. Springer Science.

Drake, D.J., C.A. Kletzing, F. Skiff, G.G. Howes, and S. Vincena. 2011. Design and use of an Elsässer probe for analysis of Alfvén wave fields according to wave direction. Rev. Sci. Instrum., 82, 103505(7), doi:10.1063/1.3649950.

Drake, D.J., J.W.R. Schroeder, G.G. Howes, C.A. Kletzing, F. Skiff, T.A Carter, and D.W. Auerbach. 2013. Alfvén wave collisions, the fundamental building block of plasma turbulence IV: laboratory experiment. Phys. Plasmas, 20, 072901(9), doi:10.1063/1.4813242.

Elsässer, W.M. 1950. The hydromagnetic equations. Phys. Rev., 79, 183.

Fuchs, V., A.K. Ram, S.D. Schultz, A. Bers, and C.N. Lashmore–Davies. 1995. Mode conversion and electron damping of the fast Alfvén wave in a tokamak at the ion-ion hybrid frequency. Phys. Plasmas, 2, 1637–1647.

Gekelman, W., H. Pfister, Z. Lucky, J. Bamber, D. Leneman, and J. Maggs. 1991. Design, construction, and properties of the large plasma device – The LaPD at UCLA. Rev. Sci. Instrum., 62, 2875–2883, doi:10.1063/1.1142175.

Gekelman, W., S. Vincena, D. Leneman, and J. Maggs. 1997. Laboratory experiments on shear Alfvén waves and their relationship to space plasmas. J. Geophys. Res., 102, 7225–7236.

Howes, G.G., D.J. Drake, K.D. Nielson, T.A. Carter, C.A. Kletzing, and F. Skiff. 2012. Toward astrophysical turbulence in the laboratory. Phys. Rev. Lett., 109, 255001(5), doi:10.1103/PhysRevLett.109.255001.

Huasen, Z. and L. Zhihong. 2013. Nonlinear generation of zonal fields by beta-induced Alfvén eigenmode in Tokamak. Plasma Sci. Technolo., 15, 969–973.

Kletzing, C.A., D.J. Thuecks, F. Skiff, S.R. Bounds, and S. Vincena. 2010. Measurements of inertial limit Alfvén wave dispersion for finite perpendicular wave number. Phys. Rev. Lett., 104, 095001(4).

Kolesnichenko, Y.I., S. Yamamoto, J. Yamazaki, V.V. Lutsenko, N. Nakajima, Y. Narushima, K. Toi, and Y.V. Yakovenko. 2004, Interplay of energetic ions and Alfvén modes in helical plasmas. Phys. Plasmas, 11, 158–170.

Leneman, D., W. Gekelman, and J. Maggs. 2006. The plasma source of the Large Plasma Device at University of California, Los Angeles. Rev. Sci. Instrum., 77, 015108(10).

Louarn, P., J.E. Wahlund, T. Chust, H. de Feraudy, A. Roux, B. Holback, P.O. Dovner, A.I. Eriksson, and G. Holmgren. 1994. Observation of kinetic Alfvén waves by the FREJA spacecraft. Geophys. Res. Lett., 21, 1847–1850, doi:10.1029/94GL00882.

Mirnov, S.V. 1964. Probe method of measuring the displacement of the current pinch in cylindrical and toroidal chambers. At. Energy, 17, 929–931.

Ogawa, K., M. Isobe, K. Toi, F. Watanabe, D.A. Spong, A. Shimizu, M. Osakabe, D.S. Darrow, S. Ohdachi, and S. Sakakibara. 2012. Magnetic configuration effects on fast ion losses induced by fast ion driven toroidal Alfvén eigenmodes in the large helical device. Plasma Sci. Technolo., 14, 269–272.

Papadopoulos, K., R.R. Sharma, and V.K. Tripathi. 1982. Parametric excitation of Alfvén waves in the ionosphere. J. Geophys. Res.: Space Phys., 87, 1491–1494.

Schroeder, J.W.R., F. Skiff, G.G. Howes, C.A. Kletzing, T.A. Carter, and S. Dorfman. 2017. Linear theory and measurements of electron oscillations in an inertial Alfvén wave. Phys. Plasmas, 24, 032902, doi:10.1063/1.4978293.

Toi, K., K. Ogawa, M. Isobe, M. Osakabe, D.A. Spong, and Y. Todo. 2011, Energetic-ion-driven global instabilities in stellarator/helical plasmas and comparison with tokamak plasmas. Plasma Phys. Control. Fus., 53, 024008, doi:10.1088/0741-3335/53/2/024008.

Tomczyk, S., S.W. McIntosh, S.L. Keil, P.G. Judges, T.S. Schad, D.H. Seeley, and J. Edmonson. 2007. Alfvén waves in the solar corona. Science, 317, 1192–1196.

Unti, T.W.J. and M. Neugebauer. 1968. Alfvén waves in the solar wind. Phys. Fluids, 11, 563–568.

U.S. Naval Research Plasma Formulary. 2019. http://www.nrl.navy.mil/ppd/content/nrl-plasma-formulary.

van der Holst, B., I.V. Sokolov, X. Meng, M. Jin, W.B. Manchester, G. Tóth, and T.I. Gombosi. 2014. Alfvén wave solar model (AWSoM): coronal heating. Astrophys. J., 782, 81–82.

Velli, M., R. Grappin, and A. Mangeney. 1989. Turbulent cascade of incompressible unidirectional Alfvén waves in the interplanetary medium. Phys. Rev. Lett., 63, 1807–1810.

Volwerk, M., P. Louarn, T. Chust, A. Roux, and H. de Feraudy. 1996. Solitary kinetic Alfvén waves: a study of the Poynting flux. J. Geophys. Res., 101, 13.335–13.343.

Yiğit, Erdal. 2017. *Atmospheric and Space Sciences: Ionospheres and Plasma Environments*. Vol 2. Springer Nature.